Photovoltaic MPPT Algorithm Based on PVT-SINC

Zhiyu Lyu, Yang Zhao, and Tianming Yu

***Abstract*—Under complex shading condition (PSC), the P-V curve of the photovoltaic (PV) array exhibits multiple peaks. This phenomenon often causes classical algorithms to become trapped at local maximum power point (LMPP). Although soft computing methods can track the global maximum power point (GMPP), their tracking speed is relatively slow. To improve the efficiency of photovoltaic systems, this paper proposes a hybrid Maximum Power Point Tracking (MPPT) algorithm that integrates power-voltage (P-V) curve tracking based on impedance matching with variable step incremental conductance (PVT-SINC). The algorithm first uses P-V curve tracking technology (PVT) to determine the GMPP and its corresponding voltage value. Then it employs variable step incremental conductance (SINC) to rapidly and precisely track the GMPP. Simulation results shows that PVT-SINC algorithms average 99.98% tracking efficiency under six cases, with average convergence times of just 0.06 seconds, which can significantly improve the PV conversion efficiency, and bring considerable economic benefits for practical engineering applications.**

***Index Terms*—photovoltaic array, boost converter, incremental conductance, partial shading condition.**

I. Introduction

WITH global development and environmental changes, the transition from conventional to renewable energy has gained widespread recognition [1]. Solar energy is regarded as a promising renewable resource due to its abundant availability, eco-friendly nature, and long-term sustainability. PV cells, which are responsible for transforming solar energy into electricity, are a key component of PV systems [2]. However, the output characteristics of PV cells are influenced by external conditions, which results in continuous shifts of the maximum power point (MPP). Additionally, partial shading caused by clouds, trees, and flocks of birds can lead to the P-V curve exhibiting multiple LMPPs and a GMPP [3]. Therefore, to ensure that the PV array consistently operates at the GMPP, it is crucial to develop an MPPT algorithm capable of adapting to complex weather conditions.

MPPT algorithms can be classified into three main categories [4]. The first category is the classical algorithms, such as Fractional Open-Circuit Voltage (FOCV) [5], Fractional Short-Circuit Current (FSCC) [6], Perturb and Observe (P&O) [7], and Incremental Conductance (INC) [8]. Although FOCV and FSCC algorithms are structurally simple, they cannot perform real-time tracking. The P&O and INC algorithms can track the MPP in real-time; however, optimizing both tracking speed and efficiency simultaneously remains a challenge. Classical algorithms are effective under stable irradiance conditions but exhibit significant performance degradation under PSC.

The second category is soft computing algorithms, such as Fuzzy Logic Control (FLC), Artificial Neural Networks (ANN), and metaheuristic algorithms [9]. Reference [10] applied FLC to MPPT by introducing a third input, beta, which expands the coverage of the membership functions in the fuzzy rules. This enhancement improves the accuracy and efficiency of the algorithm. Reference [11] proposed an ANN-based MPPT method capable of tracking the GMPP under PSC, but its generalization capability is highly dependent on training data quality. Reference [12] proposed an Improved Cuckoo Search-Golden Section Search-INC (ICS-IGSS-INC) algorithm, which combines the search capabilities of the ICS with the exploration capabilities of IGSS-INC. This approach accelerates the convergence to the GMPP under PSC. Reference [13] applied Honey Badger Algorithm (HBA) to MPPT, demonstrating accurate GMPP identification under multi-peak situation. Reference [14] proposed an improve PSO algorithm (NSNPSO-INC), which tracks the GMPP under various PSCs by combining the global search ability of NSNPSO with the fast convergence capability of INC. Although soft computing methods overcome the limitations of classical algorithms under PSC, their computational complexity results in slower tracking speeds.

The final category is P-V curve tracking algorithms, which track the P-V curves under various PSCs by modifying the DC-DC circuit structure or applying mathematical calculations. Reference [15] introduced the Spline-MPPT technique, which utilizes cubic spline interpolation to track the P-V curve and identify the GMPP. Reference [16] applied segmented cubic Hermite interpolation for MPPT to track the P-V curve, subsequently continuously tracking the GMPP using P&O method. Reference [17] introduced a high-speed MPPT module that quickly scans the P-V curve using a high-sampling-rate ADC and series inductors, then tracks the GMPP through a PI control and P&O method. Reference [18] utilized the capacitor transient phenomenon to obtain the P-V curve and then employed a PI controller for continuous GMPP tracking. While modifying the DC-DC converter topology can enhance P-V curve tracking speed compared to purely mathematical approaches, conventional circuit-based tracking algorithms typically require full curve scanning, leading to compromised tracking efficiency and additional power dissipation. To address these issues, this paper proposes a hybrid PVT-SINC algorithm that integrates

Manuscript received March 17, 2025; revised July 26, 2025.

This work was supported in part by the Science and Technology Project of Jilin Province (No.20240101354JC).

Zhiyu Lyu is an associate professor of the School of Automation Engineering, Northeast Electric Power University, Jilin, 132012, China (e-mail: lyuzhiyu1216@163.com).

Yang Zhao is a postgraduate Student of the School of Automation Engineering, Northeast Electric Power University, Jilin, 132012, China (e-mail: 2451107360@qq.com).

Tianming Yu is an associate professor of the School of Automation Engineering, Northeast Electric Power University, Jilin, 132012, China (Corresponding author e-mail: 20192928@neepu.edu.cn).

P-V curve tracking with a variable step INC algorithm. The PVT-SINC algorithm first tracks the P-V curve using impedance matching, which accelerates tracking by limiting the search space. It then further improves tracking efficiency through the variable step INC. The main contributions of this paper are as follows:

1. P-V curve tracking for PV arrays using impedance matching.
2. The algorithm accelerates the tracking process by limiting the search range of the P-V curve.
3. The proposed method introduces a variable step INC, which improves the overall performance of the algorithm by adapting the step.

II. Modeling of Photovoltaic Systems

A. Modeling of PV cells

PV cells serve as the fundamental energy conversion units in PV systems, transforming solar energy into electrical energy. Within PV cell modeling, the single-diode configurations represent the most widely utilized equivalent circuit approaches, as show in Fig. 1.

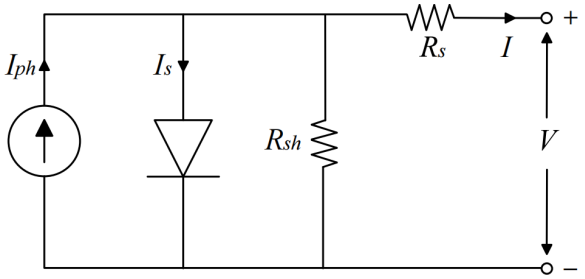

Fig. 1. Single diode PV model.

The output current I and voltage V of a PV cell can be characterized by the following expression:

$$I = I_{ph} - I_s \left\{ \exp\left[\frac{V + IR_s}{AV_T} \right] - 1 \right\} - \frac{V + IR_s}{R_{sh}} \quad (1)$$

where I_{ph} is the photocurrent, I_s is diode saturation current, R_s is the series resistance, A is the ideality factor, V_T is the thermal voltage, R_{sh} is the parallel resistance. Table I lists the detailed data of individual PV modules.

TABLE I
Parameters of PV module

Parameters	Symbols	Values
Maximum power	P_{max}	215.136W
Open circuit voltage	V_{oc}	36V
Short circuit current	I_{sc}	8.29A
Voltage at MPP	V_{mpp}	28.8V
Current at MPP	I_{mpp}	7.47A

B. Analysis of PV array output under PSC

In practical applications, the PV array typically consists of multiple solar panels. Each panel is equipped with a parallel bypass diode to prevent reverse current from damaging the array, ensuring that current flows only toward the load. Under uniform illumination, all solar panels demonstrate homogeneous performance. The bypass diodes maintain their non-conducting state under reverse bias, resulting in a single MPP.

However, under PSC, the PV panels develop mismatched P-V characteristics due to non-uniform illumination. The output current of the shaded PV cells decreases, causing the bypass diodes to activate and protect the cells. This phenomenon leads to the formation of multiple peaks in the PV array's P-V curve, complicating the identification of the true MPP. To investigate the effects of PSC on the output characteristics of PV panels, this study develops a simulation model of a PV system with three series-connected panels. The initial irradiance of the three PV modules was set to 1000 W/m², 800 W/m², and 400 W/m² at a constant temperature of 25°C. Fig. 2 shows the output characteristics under these conditions. Due to the differing irradiance levels across the three PV panels, three distinct peak points appeared. This shows that under PSC, both the number of peak points and the GMPP of the PV array's output power curve are significantly influenced by the irradiance levels.

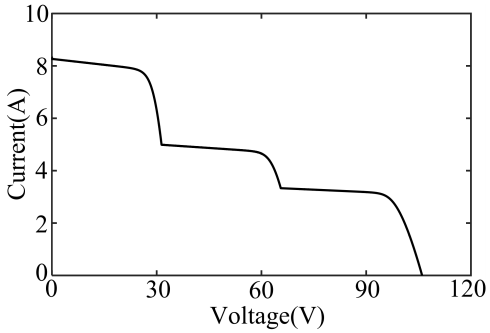

(a) I-V curve

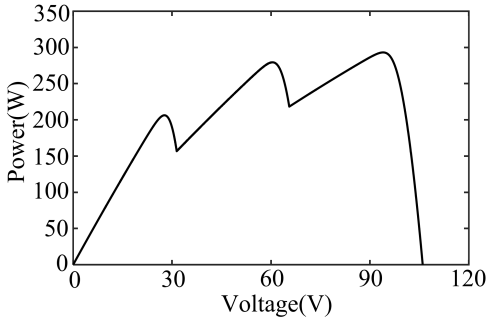

(b) P-V curve

Fig. 2. Photovoltaic P-V and I-V curves under PSC.

III. MPPT Algorithm Based on PVT-SINC

A. P-V curve tracking

The proposed PVT technique operates by matching the PV array's impedance with the connected load resistance. The PV system changes the impedance of the PV array by adjusting the duty cycle of the boost converter, thereby altering the operating point of the PV array. This impedance matching principle defines the operational characteristics:

1. Decreased load resistance drives the PV system into a high-current operational regime with concomitantly reduced voltage output.

2. Increased load resistance forces the PV system into a high-voltage operational regime with concomitantly diminished current output.

By tracking the PV array's P-V curve across varying impedances (from low to high), the GMPP and its corresponding voltage values (V_{mpp}) can be accurately and quickly determined.

To reduce the P-V curve search space, the lower limit (R_{min}) and upper limit (R_{max}) of the PV array's impedance are calculated. Given that $I_{mpp,stc}$ is the maximum current of the PV array at GMPP, the R_{min} calculated by Eq. (2) is lower than the impedance at the GMPP of the PV array [19]. Additionally, V_{mpp} is less than $0.9V_{oc,stc}$. As a result, the R_{max} calculated by Eq. (3) serves as the upper impedance limit for the PV array at the GMPP [20]. The impedance at the GMPP is constrained within the range of R_{min} to R_{max}. Therefore, identifying the GMPP requires only searching the P-V curves within this limited impedance range. This method effectively reduces the search space and enhances the efficiency of the GMPP search process.

$$R_{min} = \frac{P_{GMPP}}{I_{mpp,stc}^2} \tag{2}$$

$$R_{max} = \frac{(0.9 \times V_{oc,stc})^2}{P_{GMPP}} \tag{3}$$

where $I_{mpp,stc}$ is the current of the PV array at the GMPP under standard test conditions (STC), P_{GMPP} is the maximum power value, $V_{oc,stc}$ is the open-circuit voltage of the PV array under STC.

Fig. 3 shows the PV system used to validate the proposed MPPT technique. The system includes a PV array with three series-connected modules. The DC-DC conversion circuit employs a boost converter topology, with an additional switch (S_b) and resistor (R) connected in series after the inductor. In this study, the PV modules are subjected to irradiance levels ranging from 200 W/m² to 1000 W/m². According to Eq. (2) and Eq. (3), the PV array exhibits impedance values ranging from 2 Ω to 73 Ω.

When the GMPP shifts under varying irradiance conditions, the procedure for tracking the P-V curve using the PVT is as follows:

(1) The boost circuit switch S_b is turned off, and switch S_c is turned on. During this period, the PV array's output voltage decreases, and the output current increases, as shown in Fig. 4 (5-11ms).
(2) When the impedance of the PV array is observed to fall below the lower limit (R_{min}), S_c is turned off and S_b is turned on. This control action leads to an impedance increase, accompanied by a voltage rise and current reduction, as shown in Fig. 4 (11ms-27ms).
(3) When the PV array's impedance exceeds the upper limit (R_{max}), the P-V curve tracking phase terminates. The SINC algorithm subsequently initiates GMPP tracking, as shown in Fig. 4 (27ms-50ms).

B. Variable step INC

The INC algorithm iteratively perturbs the PV array's operating voltage while observing the power change, and adjusts the duty cycle to track the MPP. The core

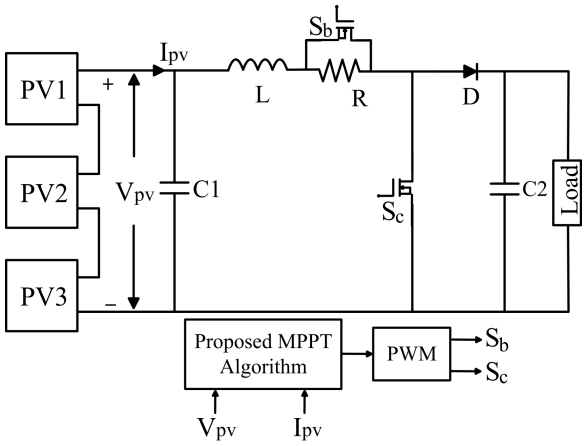

Fig. 3. The proposed PVT operation methodology.

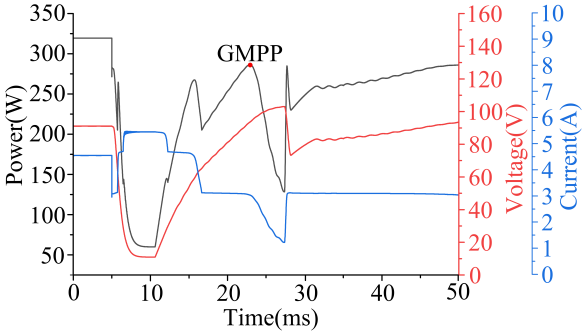

Fig. 4. PV array V_{pv}, I_{pv}, and P_{pv} curves under PSC.

principle lies in locating the operating point by comparing instantaneous conductance with incremental conductance, then dynamically adjusting the voltage perturbation direction. The INC algorithm's operational steps are as follows:

Step 1: Measure the current voltage V and current I of the PV array in real-time.

Step 2: Calculate the conductance value G according to Eq. (4).

$$G = \frac{dI}{dV} \tag{4}$$

Step 3: Calculate the amount of change in conductance according to Eq. (5).

$$\Delta G = G(K) - G(K-1) \tag{5}$$

where $G(K)$ and $G(K-1)$ are the PV array conductance at time K and $K-1$, respectively.

Step 4: If $\Delta G > 0$, the operating point is located on the left side of the MPP, requiring a positive voltage adjustment; if $\Delta G < 0$, it indicates a right-side position necessitating a negative voltage correction; if $\Delta G = 0$, it indicates that the current working point is at MPP and no change is needed.

The INC algorithm adopts a fixed step and cannot dynamically adjust the step according to the actual operating state of the PV system. To overcome this limitation, this study proposes a variable step INC algorithm that dynamically adjusts the step based on the optimal voltage of the PV array.

$$\Delta D = \begin{cases} \Delta D_1 & 0.95 \times V_{mpp} \le V_{pv} \le 1.05 \times V_{mpp} \\ \Delta D_2 & \text{else} \end{cases} \tag{6}$$

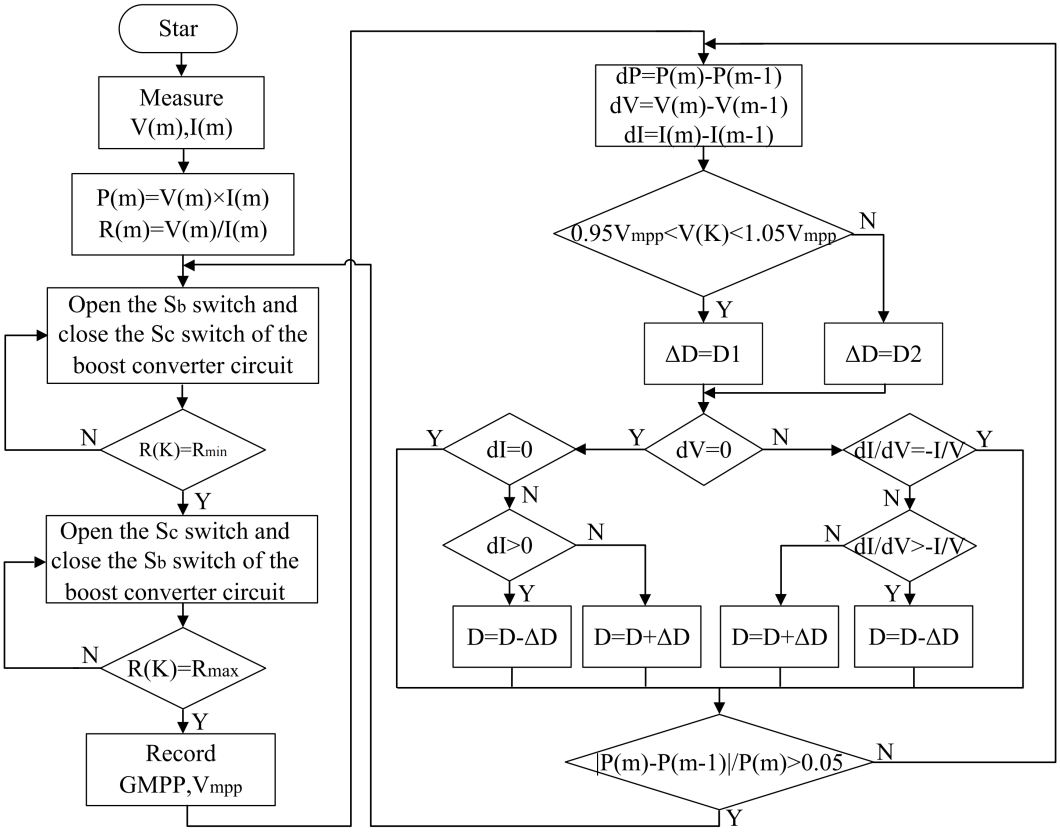

Fig. 5. Overall control flow of the PVT-SINC algorithm.

where ΔD is the perturbation step, $\Delta D1$ is a small step, $\Delta D2$ is a large step, V_{pv} is the PV array's output voltage. When V_{pv} is far from V_{mpp}, a larger step $\Delta D2$ is used to accelerate the MPPT. Otherwise, when the working point is near to the GMPP, a smaller step $\Delta D1$ is used to perturb the operating voltage. The SINC algorithm achieves higher tracking accuracy near the PV array's optimal operating voltage. Consequently, it simultaneously reduces steady-state voltage oscillations and accelerates maximum power point tracking convergence.

C. PVT-SINC algorithm

The PVT-SINC algorithm integrates the advantages of fast P-V curve tracking with the rapid convergence and high accuracy of the SINC algorithm. Initially, the PVT is utilized to trace the P-V curve. Upon completion of this tracking process, the values corresponding to the GMPP and its voltage (V_{mpp}) are recorded. Thereafter, the algorithm transitions to the SINC algorithm. At this stage, the SINC algorithm adjusts the step to ensure rapid and precise stabilization at the GMPP.

To ensure that PVT-SINC algorithm can smoothly switch to the SINC algorithm when the PV curve tracking is completed, Eq. (7) is used to determine whether the algorithm switching condition is satisfied.

$$0 = R_{pv} - R_{max} \tag{7}$$

where R_{pv} is the PV array impedance, R_{max} is the upper limit of the PV array impedance. When the condition specified in Eq. (7) is satisfied, this indicates that the P-V curve tracking process has been successfully completed. At this stage, the PVT-SINC algorithm transitions seamlessly to the SINC algorithm, which is then activated to track the GMPP.

In addition, when the external environment changes, the algorithm calculates the power variation (ΔP) to determine whether the MPPT needs to be restarted to prevent power loss.

$$\Delta P = \left| \frac{P(m) - P(m-1)}{P(m)} \right| > 0.05 \tag{8}$$

where $P(m)$ is the power of the PV system at time m, and $P(m-1)$ is the power at the previous time step $(m-1)$. When $\Delta P > 0.05$, restart the MPPT; otherwise, continue tracking with the SINC algorithm.

The control flow of the PVT-SINC algorithm is shown in Fig. 5, and the corresponding operation steps are as follows:

Step 1: Close switch S_c, disconnect switch S_b, measure the voltage and current of the PV array, and calculate its internal resistance R_{pv}.

Step 2: Compare R_{pv} with R_{min}; if $R_{pv} = R_{min}$, proceed to the next step; otherwise, return to and continue to execute step 1.

Step 3: Close switch S_b, disconnect switch S_c, and calculate R_{pv}.

Step 4: Compare R_{pv} with R_{max}; if $R_{pv} > R_{max}$, proceed to the next step; otherwise, return to and continue to execute step 3.

Step 5: Record the GMPP and its corresponding optimal voltage value.

Step 6: Engage the SINC algorithm to maintain operation at the GMPP.

Step 7: Determine whether the algorithm needs to be restarted according to Eq. (8); if the restart condition is met, return to Step 1; otherwise, proceed to Step 6.

IV. Algorithm Simulation and Analysis

MATLAB/Simulink was used to design a photovoltaic system, as shown in Fig. 3, to examine the efficiency of the PVT-SINC algorithm. The PV array consists of three series-connected PV modules, with the detailed data provided in Table I. The component specifications of the boost converter include C1=470uF, C2=47uF, L=0.5mH, R=2Ω, and Load=90Ω.

To verify the performance of the PVT-SINC algorithm, this study sets up six lighting conditions covering four typical application scenarios: uniform irradiation scenario, weak shadowing scenario, strong shadowing scenario, and dynamic shadowing scenario. Under the uniform irradiation condition, all PV modules receive equal irradiation intensity and only a single GMPP exists, as shown in Case1 of Fig. 6. Under the weak shadowing condition, one PV module is shaded while the others remain fully illuminated, which produces one LMPP and one GMPP, as shown in Case2 of Fig. 6. Under the strong shadowing condition, all three PV modules are partially shaded, resulting in two LMPPs and one GMPP, as shown in Case3 of Fig. 6. Under the dynamic shadowing condition, the irradiation intensity of the three PV modules transitions from Case4 to Case6 in Fig. 6, aiming to test the algorithm's ability to track GMPP under time-varying irradiation. The irradiation intensity parameters for each scenario are listed in Table II.

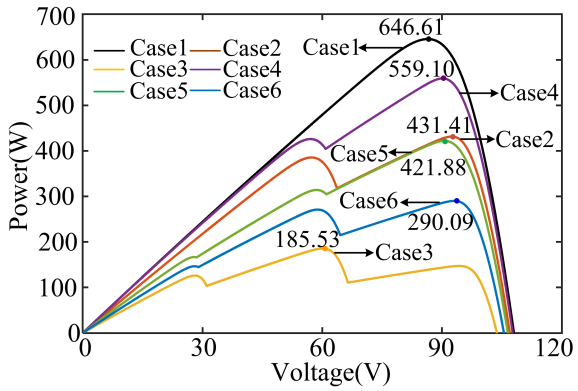

Fig. 6. P-V curves of PV arrays under Cases 1-6.

TABLE II
PV Module Irradiance Values in Different Cases

Case	Irradiance(W/m^2)			GMPP(W)
	PV1	PV2	PV3	
Case1	1000	1000	1000	645.61
Case2	900	900	600	431.41
Case3	600	400	200	185.53
Case4	1000	1000	800	559.10
Case5	800	700	600	421.88
Case6	700	600	400	290.09

A. Uniform irradiation condition

Under the uniform irradiance condition, all PV panels receive the same 1000 W/m² irradiation, leading to a GMPP of 646.25 W for the PV array. Since the illumination is uniformly distributed, the P-V curve exhibits only a single peak power point.

Fig. 7 presents the simulation results of the four algorithms under the uniform irradiation condition. The PVT-SINC, HBA, NSNPSO-INC, and PSO algorithms track power values of 645.40 W, 645.19 W, 645.37 W, and 645.05 W, respectively, with corresponding tracking times of 0.06 s, 0.45 s, 0.15 s, and 0.85 s. The simulation results under the uniform illumination condition show that the PVT-SINC algorithm outperforms the other three algorithms in terms of tracking speed and efficiency. This is because PSO, NSNPSO-INC, and HBA algorithms require multiple iterations to search for and localize the GMPP. In contrast, the PVT-SINC algorithm quickly scans the P-V curve using the PVT module. Once the search stage is complete, the algorithm can rapidly and accurately track the GMPP with the SINC module, significantly improving its response speed and tracking accuracy.

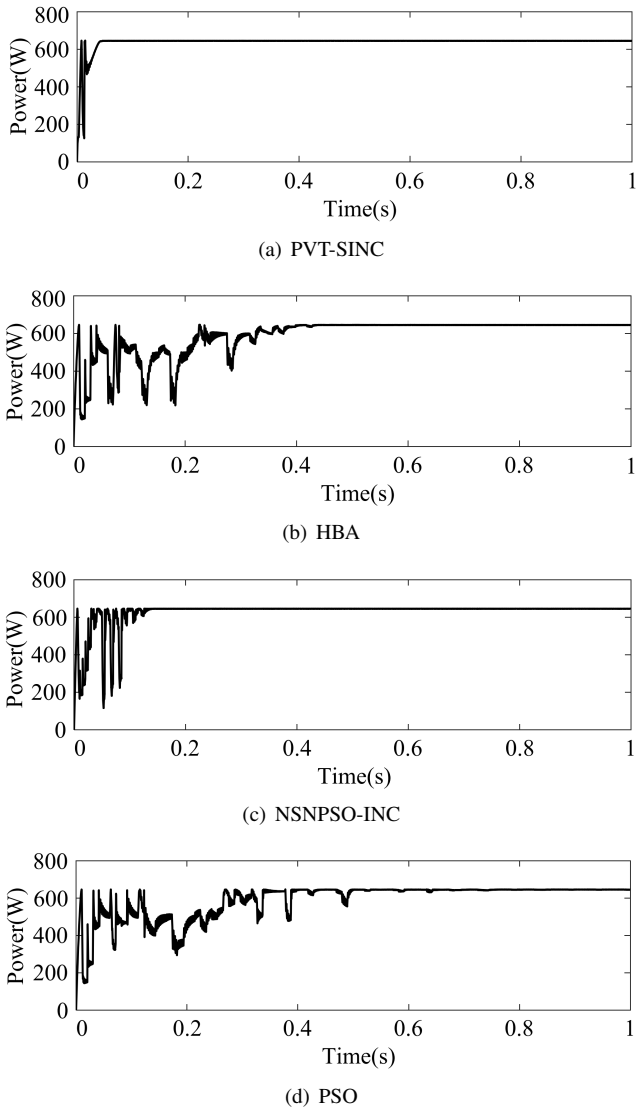

(a) PVT-SINC

(b) HBA

(c) NSNPSO-INC

(d) PSO

Fig. 7. Simulation results under the uniform irradiation condition.

B. Weak shadowing condition

Under the weak shadowing condition, only one PV panel is shaded, while the others are in uniformly illuminated environment. The specific parameters are provided in Case2 of Table II. In this scenario, the P-V curve exhibits two power peaks, with the GMPP located on the right side at 431.41 W.

The simulation comparison results of the four algorithms under the weak shadowing condition are shown in Fig. 8. The final tracking powers for the PVT-SINC, HBA, NSNPSO-INC, and PSO algorithms are 431.33 W, 431.31 W, 431.30 W, and 431.23 W, respectively, with corresponding tracking times of 0.07 s, 0.48 s, 0.18 s, and 0.66 s. The PSO, HBA, and NSNPSO-INC algorithms must search for the GMPP on power curves containing local peaks. This process requires evaluating and differentiating each power point to avoid local optima. As a result, these algorithms require more iterations and exhibit slower convergence. In contrast, the PVT-SINC algorithm quickly identifies the LMPP and GMPP at the initial stage by scanning the P-V curve using the PVT module, enabling fast and accurate power tracking. Even under the complex, non-linear power output condition caused by shading, the PVT-SINC algorithm maintains excellent tracking speed and efficiency.

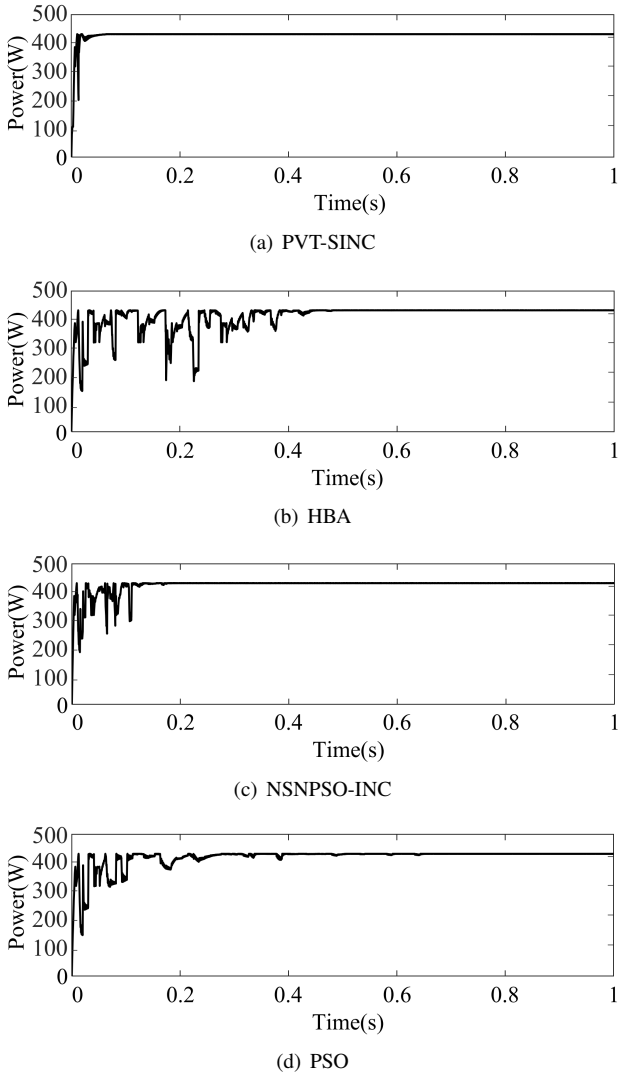

(a) PVT-SINC

(b) HBA

(c) NSNPSO-INC

(d) PSO

Fig. 8. Simulation results under the weaker shadowing condition.

C. Strong shadowing condition

Under the strong shadowing condition, all PV panels are shaded, and the irradiation intensity varies across the panels. The specific parameters are provided in Case3 of Table II. Under this condition, the P-V curves exhibit three power peaks, with the GMPP located in the middle at 185.53 W.

The simulation comparison results of the four algorithms under the strong shadowing condition are shown in Fig. 9. The tracking powers for the PVT-SINC, HBA, NSNPSO-INC, and PSO algorithms are 185.48 W, 185.48 W, 185.47 W, and 185.41 W, respectively, with corresponding tracking times of 0.05 s, 0.49 s, 0.14 s, and 0.65 s. Due to the presence of multiple local peaks, the PSO and HBA algorithms exhibit longer tracking times and significant power fluctuations during the search process, leading to power losses. By integrating the INC method, the NSNPSO-INC algorithm demonstrates a significant improvement in tracking speed. The PVT-SINC algorithm achieves the fastest tracking speed while ensuring the tracking efficiency. The simulation results under the strong shadowing condition demonstrate that the PVT-SINC algorithm achieves excellent convergence speed and tracking accuracy,while maintaining robust performance and dynamic response capability in complex occlusion environments.

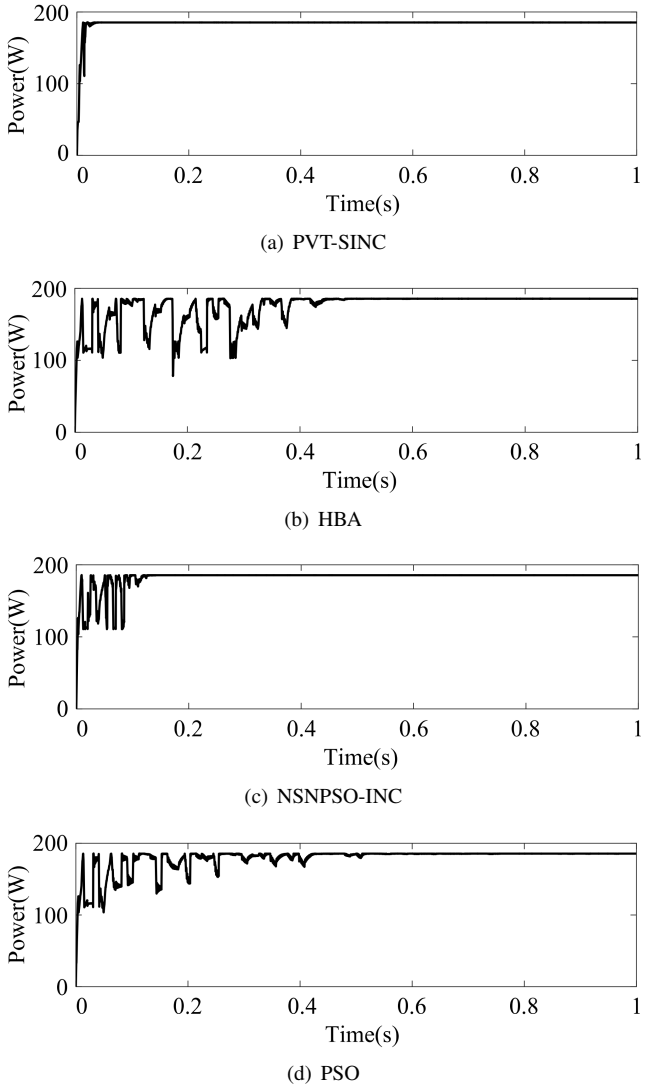

(a) PVT-SINC

(b) HBA

(c) NSNPSO-INC

(d) PSO

Fig. 9. Simulation results under the strong shadowing condition.

Table III presents the simulation results of four algorithms under static lighting conditions. The average tracking power values for the PVT-SINC, HBA, NSNPSO-INC, and PSO algorithms were 420.74 W, 420.66 W, 420.71 W, and 420.56 W, respectively, while their average tracking times were 0.06 s, 0.47 s, 0.16 s, and 0.71 s, respectively. These results demonstrate the PVT-SINC algorithm's superior tracking efficiency and faster convergence compared to the other three algorithms.

TABLE III
COMPARISON OF SIMULATION RESULTS OF FOUR ALGORITHMS UNDER STATIC LIGHTING CONDITION

Case	Algorithm	Power tracked(W)	Tracking time(s)	Efficiency(%)
Uniform irradiance	PVT-SINC	645.40	0.06	99.97
	HBA	645.19	0.45	99.93
	NSNPSO-INC	645.37	0.15	99.96
	PSO	645.05	0.81	99.91
Weak shadowing	PVT-SINC	431.33	0.07	99.98
	HBA	431.31	0.48	99.98
	NSNPSO-INC	431.30	0.18	99.97
	PSO	431.23	0.66	99.96
Strong shadowing	PVT-SINC	185.48	0.05	99.97
	HBA	185.48	0.49	99.97
	NSNPSO-INC	185.47	0.14	99.97
	PSO	185.41	0.65	99.94

D. Dynamic shadowing condition

Under the dynamic shadowing condition, the PV array undergoes three different irradiance stages. The simulation runs for 3 seconds, with shadows changing every second, corresponding to the irradiation levels in Cases 4, 5, and 6 in Fig. 6. These shadowing scenarios are detailed in Table II. This simulation aims to assess the re-optimization capability of the PVT-SINC algorithm under dynamic environment.

Fig. 10 presents the simulation results of the four algorithms under the dynamic shadowing condition. The average tracking powers of the PVT-SINC, HBA, NSNPSO-INC, and PSO algorithms are 423.61 W, 416.96 W, 423.55 W, and 407.01 W, respectively, with corresponding average tracking times of 0.05 s, 0.49 s, 0.15 s, and 0.72 s. The PSO and HBA algorithms exhibit significant fluctuations in output power during the tracking process, resulting in slower overall convergence. Specifically, the PSO algorithm struggles to accurately track the GMPP during the third stage, whereas the HBA algorithm converges prematurely in this stage, leading to a local optimum and failure to reach the GMPP. Additionally, the NSNPSO-INC algorithm successfully tracks the GMPP at each stage, but it still suffers from slow tracking speed. The PVT-SINC algorithm efficiently re-searches the GMPP when the irradiance intensity changes, achieving the fastest tracking speed and optimal efficiency. This is primarily attributed to its search space restriction mechanism, which enables rapid localization of the GMPP by narrowing the search range.

Table IV presents the simulation results of the PVT-SINC, HBA, NSNPSO-INC, and PSO algorithms under the dynamic shadowing condition. The simulation results indicate that the PVT-SINC algorithm exhibits faster tracking speed, higher efficiency, and less oscillation under dynamically changing irradiance condition.

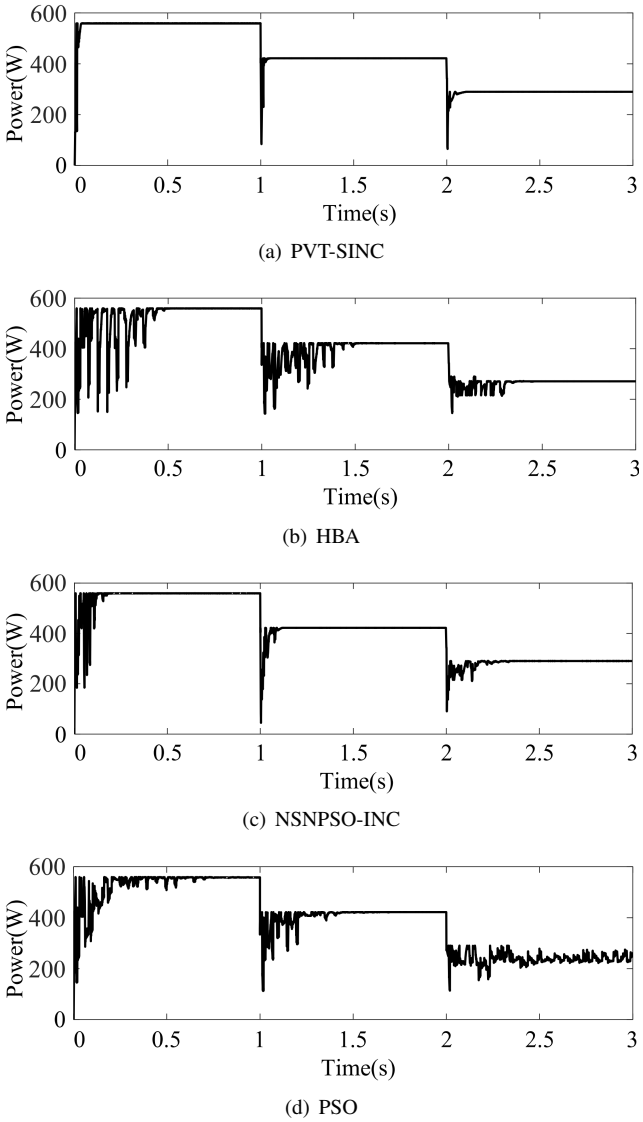

(a) PVT-SINC

(b) HBA

(c) NSNPSO-INC

(d) PSO

Fig. 10. Simulation results under dynamic shadowing condition.

TABLE IV
COMPARISON OF SIMULATION RESULTS OF FOUR ALGORITHMS UNDER DYNAMIC SHADOWING CONDITION

Stage	Algorithm	Power tracked(W)	Tracking time(s)	Efficiency(%)
Stage1	PVT-SINC	558.97	0.05	99.98
	HBA	558.95	0.51	99.97
	NSNPSO-INC	558.89	0.19	99.96
	PSO	558.18	0.76	99.84
Stage2	PVT-SINC	421.79	0.06	99.98
	HBA	421.28	0.48	99.86
	NSNPSO-INC	421.70	0.12	99.96
	PSO	421.78	0.66	99.98
Stage3	PVT-SINC	290.07	0.05	99.99
	HBA	270.64	0.47	93.29
	NSNPSO-INC	290.06	0.14	99.99
	PSO	241.06	0.73	83.09

V. Conclusions

This paper proposes a MPPT control algorithm named PVT-SINC, which combines the P-V curve tracking with a variable step incremental conductance algorithm. The algorithm dynamically switches between PVT and SINC modes, enabling stable tracking of the GMPP under various PSCs. Four different weather conditions are simulated, and compares the effectiveness of the PVT-SINC algorithm with that of the HBA, NSNPSO-INC, and PSO algorithms. The simulation results show that the PVT-SINC algorithm achieves an average tracking efficiency of 99.98% across six cases, with an average tracking time of only 0.06 seconds. The overall performance of the PVT-SINC algorithm is better than the HBA, NSNPSO-INC, and PSO algorithms, effectively tracking the GMPP with fast tracking speed, minimal power fluctuations, and robust adaptability.

References

[1] B. M. Opeyemi, "Path to sustainable energy consumption: The possibility of substituting renewable energy for non-renewable energy," *Energy*, vol. 228, pp. 1–9, 2021.

[2] X. Ru, "An Improved Butterfly Optimization Algorithm for Numerical Optimization and Parameter Identification of Photovoltaic Model," *Engineering Letters*, vol. 33, no. 1, pp. 169–184, 2025.

[3] M. Kumar, K. P. Panda, J. C. Rosas-Caro, A. Valderrabano-Gonzalez, and G. Panda, "Comprehensive Review of Conventional and Emerging Maximum Power Point Tracking Algorithms for Uniformly and Partially Shaded Solar Photovoltaic Systems," *IEEE Access*, vol. 11, pp. 31 778–31 812, 2023.

[4] M. Y. Worku, M. A. Hassan, L. S. Maraaba, M. Shafiullah, M. R. Elkadeem, M. I. Hossain, and M. A. Abido, "A Comprehensive Review of Recent Maximum Power Point Tracking Techniques for Photovoltaic Systems under Partial Shading," *Sustainability*, vol. 15, no. 14, pp. 1–28, 2023.

[5] A. Hassan, O. Bass, and M. A. S. Masoum, "An improved genetic algorithm based fractional open circuit voltage MPPT for solar PV systems," *Energy Reports*, vol. 9, pp. 1535–1548, 2023.

[6] C. B. N. Fapi, P. Wira, M. Kamta, H. Tchakounté, and B. Colicchio, "Simulation and dSPACE Hardware Implementation of an Improved Fractional Short-Circuit Current MPPT Algorithm for Photovoltaic System," *Applied Solar Energy*, vol. 57, no. 2, pp. 93–106, 2021.

[7] S. F. Chevtchenko, E. J. Barbosa, M. C. Cavalcanti, G. M. Azevedo, and T. B. Ludermir, "Combining PPO and incremental conductance for MPPT under dynamic shading and temperature," *Applied Soft Computing*, vol. 131, pp. 1–14, 2022.

[8] L. Shang, H. Guo, and W. Zhu, "An improved MPPT control strategy based on incremental conductance algorithm," *Protection and Control of Modern Power Systems*, vol. 5, no. 1, pp. 1–8, 2020.

[9] M. Mao, L. Cui, Q. Zhang, K. Guo, L. Zhou, and H. Huang, "Classification and summarization of solar photovoltaic MPPT techniques: A review based on traditional and intelligent control strategies," *Energy Reports*, vol. 6, pp. 1312–1327, 2020.

[10] R. Bisht and A. Sikander, "An improved method based on fuzzy logic with beta parameter for PV MPPT system," *Optik*, vol. 259, pp. 1–13, 2022.

[11] A. F. Abouzeid, H. Eleraky, A. Kalas, R. Rizk, M. M. Elsakka, and A. Refaat, "Experimental validation of a low-cost maximum power point tracking technique based on artificial neural network for photovoltaic systems," *Scientific Reports*, vol. 14, no. 1, pp. 1–22, 2024.

[12] Tan Liu, Hexu Yu, Sisi Liu, Jiaqi Tong, Zhiyi Wu, and Qingyun Yuan, "Photovoltaic MPPT Tracking under Partial Shading Based on ICS-IGSS-INC Hybrid Algorithm," *Engineering Letters*, vol. 33, no. 2, pp. 215–222, 2025.

[13] Qianjin Gui, Lei Wang, Chao Ding, Wenfa Xu, Xiaoyang Li, Feilong Yu, and Haisen Wang, "Multi-Peak Photovoltaic Maximum Power Point Tracking Method Based on Honey Badger Algorithm Under Localized Shading Conditions," *Energies*, vol. 18, no. 5, pp. 1–14, 2025.

[14] S. Z. Xu and Y. M. Zhong, "NSNPSO-INC: A Simplified Particle Swarm Optimization Algorithm for Photovoltaic MPPT Combining Natural Selection and Conductivity Incremental Approach," *IEEE Access*, vol. 12, pp. 137 760–137 774, 2024.

[15] A. Ostadrahimi and Y. Mahmoud, "Novel Spline-MPPT Technique for Photovoltaic Systems Under Uniform Irradiance and Partial Shading Conditions," *IEEE Transactions on Sustainable Energy*, vol. 12, no. 1, pp. 524–532, 2021.

[16] C. Yuan, J. Xia, F. Huang, P. Zhao, and L. Kong, "A Novel Hermite Interpolation-Based MPPT Technique for Photovoltaic Systems Under Partial Shading Conditions," *IEEE Photonics Journal*, vol. 16, no. 2, pp. 1–10, 2024.

[17] S. Selvakumar, M. Madhusmita, C. Koodalsamy, S. P. Simon, and Y. R. Sood, "High-Speed Maximum Power Point Tracking Module for PV Systems," *IEEE Transactions on Industrial Electronics*, vol. 66, no. 2, pp. 1119–1129, 2019.

[18] S. S. Sakthivel, V. Arunachalam, S. P. P, and S. K, "Improved Global Maximum Power Point Tracking Technique for a Partially Shaded Solar Photovoltaic Array Using Capacitor Transient Effect," *IEEE Transactions on Industrial Informatics*, vol. 20, no. 12, pp. 13 853–13 862, 2024.

[19] A. M. S. Furtado, F. Bradaschia, M. C. Cavalcanti, and L. R. Limongi, "A Reduced Voltage Range Global Maximum Power Point Tracking Algorithm for Photovoltaic Systems Under Partial Shading Conditions," *IEEE Transactions on Industrial Electronics*, vol. 65, no. 4, pp. 3252–3262, 2018.

[20] S. Xu, Y. Gao, G. Zhou, and G. Mao, "A Global Maximum Power Point Tracking Algorithm for Photovoltaic Systems Under Partially Shaded Conditions Using Modified Maximum Power Trapezium Method," *IEEE Transactions on Industrial Electronics*, vol. 68, no. 1, pp. 370–380, 2021.